

First-principles study on the magnetic and electronic properties of the high-pressure orthorhombic phase of MnSe

Xiao-Xiao Man , Ben-Chao Gong , Pei-Han Sun , Kai Liu *, and Zhong-Yi Lu †

Department of Physics and Beijing Key Laboratory of Opto-electronic Functional Materials & Micro-nano Devices, Renmin University of China, Beijing 100872, China



(Received 26 August 2021; revised 2 July 2022; accepted 6 July 2022; published 20 July 2022)

Exploring the mechanism of unconventional superconductivity has been one of the most important topics in condensed matter physics, while studying the magnetic and electronic properties of the parent compounds of unconventional superconductors can provide helpful clues. Recently, superconductivity in the orthorhombic-phase MnSe was successfully induced by applying high pressure, which makes MnSe the second Mn-based superconductor after MnP. Based on the spin-polarized density functional theory calculations, we have studied the magnetic and electronic properties of the orthorhombic-phase MnSe under high pressure. We show that there may exist strong antiferromagnetic (AFM) fluctuations in a narrow energy window (less than 3 meV/Mn) among an AFM state dubbed AFM3 and a series of staggered n -mer AFM states. Here the n -mer means that a set of n adjacent spins on a line are parallelly aligned. In the AFM3 state and the n -mer AFM states, the Mn spins show AFM coupling along the x axis and ferromagnetic (FM) coupling along the y axis, but respectively host FM and staggered n -mer AFM correlations along the z axis. Our calculations indicate that the orthorhombic-phase MnSe exhibits a metallic behavior in the low-energy magnetic states, in good accordance with the previous experimental observations. We also map the calculated energies onto an effective Heisenberg model and obtain the exchange couplings J , whose values can serve as a reference for analyzing the data from magnetic measurements. Two usual mechanisms like Fermi surface nesting and electron-phonon coupling can be ruled out as the origin of superconductivity. The magnetic properties in the orthorhombic-phase MnSe under high pressure need future in-depth experimental examination.

DOI: [10.1103/PhysRevB.106.035136](https://doi.org/10.1103/PhysRevB.106.035136)

I. INTRODUCTION

Investigating the origin of unconventional superconductivity has been one of the most important subjects in condensed matter physics. While the parent compounds of unconventional superconductors often show long-range magnetic orders, the unconventional superconductivity could be induced by suppressing the static magnetic orders via external pressure [1–4] or charge doping [5–12]. As a result, studying the magnetic and electronic properties of the parent compounds of unconventional superconductors can provide important clues for the underlying superconducting mechanism. Generally, the parent compounds of cuprate superconductors are Mott insulators with the antiferromagnetic (AFM) Néel order in the CuO_2 plane [13–15] due to the strong correlation among $\text{Cu-}3d$ electrons. In comparison, most parent compounds of iron-based superconductors show single-stripe (collinear) AFM order in the FeSe(As) layer and are semimetals with moderate electronic correlation [16–24]. Among these materials, unconventional superconductivity is closely related to magnetic instability.

Beyond the two families of cuprate and iron-based superconductors, it is natural to search for other $3d$ magnetic

compounds which can be superconducting and to investigate their magnetic and electronic properties. Recently, an Mn-based superconductor MnP was discovered and it develops an AFM-type magnetic order at low temperature before becoming superconducting under pressure [25,26]. Both the low-pressure and high-pressure magnetic phases of MnP were well described by the first-principles calculations [27,28]. In last year, Hung *et al.* demonstrated that the high pressure can also induce superconductivity in MnSe [29], namely the second Mn-based superconductor after MnP. At normal conditions, MnSe adopts a cubic NaCl-type structure [30] and exhibits a semiconducting behavior with a band gap of 2.0 eV [31]. It undergoes a cubic (NaCl-type) to orthorhombic (MnP-type) phase transition when the pressure increases to 20–30 GPa [29], which also accompanies a transition of Mn^{2+} from a high-spin ($S = 5/2$) state to a low-spin ($S = 1/2$) state as well as metallization [32]. Hung *et al.* then observed superconductivity in MnSe with T_c of 5 K at ~ 12 GPa and the highest T_c of 9 K at ~ 35 GPa [29], and they suggested that the pressure can suppress the AFM transition above ~ 26 GPa [29]. Correspondingly, the magnetic properties and electronic structure of MnSe at high pressure need theoretical elucidation.

In this work, we employed the first-principles electronic structure calculations to investigate the magnetic and electronic properties of the orthorhombic-phase MnSe under high pressure. We show that there are likely strong

*kliu@ruc.edu.cn

†zlu@ruc.edu.cn

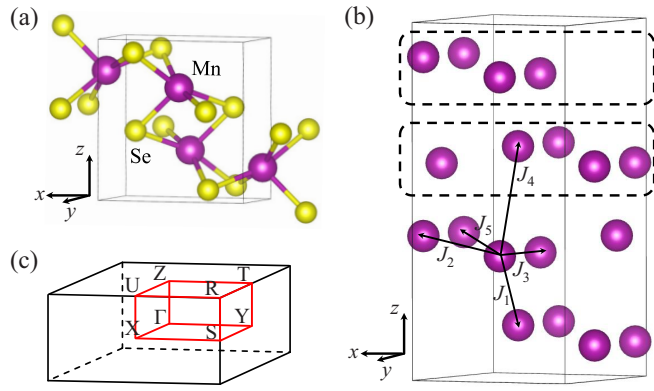


FIG. 1. (a) Crystal structure of the orthorhombic-phase (MnP-type) MnSe under 30 GPa. (b) Schematics of the exchange interactions between the Mn spins. Here, the dashed rectangle frames represent the different Mn layers. The nearest-neighboring (NN) J_1 , next-nearest-neighboring (NNN) J_2 , third NN J_3 , fourth NN J_4 , and fifth NN J_5 are labeled. (c) Brillouin zone (BZ) of the orthorhombic-phase MnSe. The high-symmetry paths in the BZ are indicated by the red lines.

antiferromagnetic fluctuations in a narrow energy window (less than 3 meV/Mn) among an AFM state dubbed AFM3 and a series of staggered n -mer AFM states that we named. Compared with the semiconducting character of the cubic phase, the orthorhombic phase of MnSe exhibits a metallic

behavior in the AFM3 magnetic state, which is in accordance with the previous experimental observations [29].

II. COMPUTATIONAL DETAILS

The first-principles electronic structure calculations on MnSe were carried out by using the projector augmented wave (PAW) method [33,34] as implemented in the VASP package [35–37]. The generalized gradient approximation (GGA) of the Perdew-Burke-Ernzerhof (PBE) type [38] was adopted for the exchange-correlation functional. The kinetic energy cutoff of the plane-wave basis was set to 500 eV. For the orthorhombic-phase (MnP-type) MnSe, the lattice constants were fixed to the experimental values at high pressure ($P = 30$ GPa: $a = 5.7527$ Å, $b = 3.1045$ Å, and $c = 6.0434$ Å) [29]. The nonmagnetic (NM), ferromagnetic (FM), and several antiferromagnetic (AFM) states were studied with a $1 \times 2 \times 1$ supercell and a $12 \times 10 \times 12$ \mathbf{k} -point mesh for the Brillouin zone sampling, while other staggered n -mer AFM states were investigated with the larger supercells (Fig. 2). The maximally localized Wannier functions method [39,40] was used to calculate the Fermi surface. As to the cubic-phase (NaCl-type) MnSe, the lattice constants were fixed at the experimental values of $a = b = c = 5.4630$ Å [30] and the magnetic structure determined by the neutron powder diffraction (NPD) measurement [41] was adopted. Since the GGA functional fails to describe the semiconducting behavior [31] of the cubic-phase MnSe, we performed the GGA + U calculations based on the scheme of Dudarev *et al.* [42] respectively with the effective

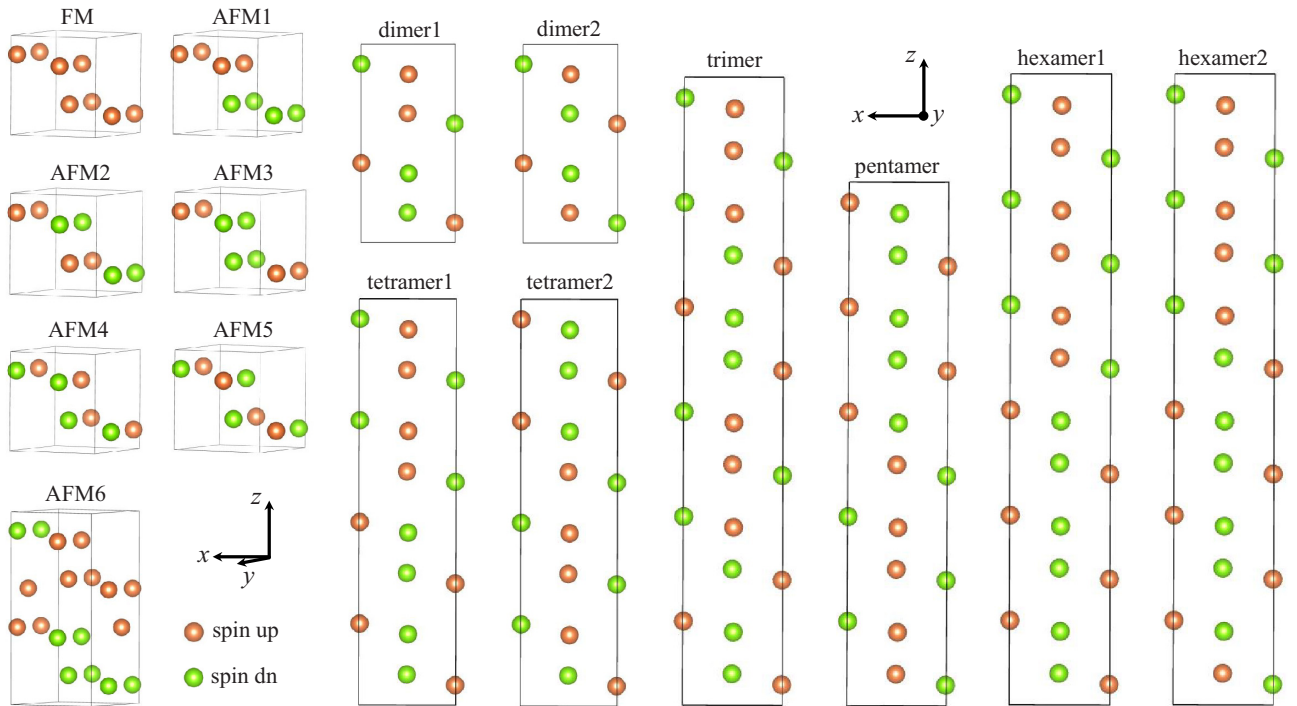


FIG. 2. Sketches of various magnetic configurations for the Mn lattice of the orthorhombic-phase MnSe under 30 GPa. Here, the solid cubes and rectangles represent the supercells, while the orange and green balls represent the spin-up and spin-down Mn atoms, respectively. The n -mer magnetic states are all composed of the staggered n -mer chain lying along the z direction and the same (different) spin polarization along the y (x) direction. Here the side views of the magnetic patterns for the dimer ($n = 2$), trimer ($n = 3$), tetramer ($n = 4$), pentamer ($n = 5$), and hexamer ($n = 6$) states are demonstrated.

TABLE I. Relative energies ΔE (in units of meV/Mn) of various magnetic states with respect to the NM state for the orthorhombic-phase MnSe calculated with the fixed lattice constants [29] and relaxed internal atomic positions under the GGA level at 30 GPa. The corresponding average local moments \bar{M} (in units of μ_B) on Mn atoms are also listed.

State	NM	FM	AFM1	AFM2	AFM3	AFM4	AFM5	AFM6
ΔE	0.00	-84.08	-112.87	-182.29	-192.02	-74.45	-118.61	-172.66
\bar{M}	—	1.84	1.78	2.21	2.13	2.02	2.07	2.06
State	dimer1	dimer2	trimer	tetramer1	tetramer2	pentamer	hexamer1	hexamer2
ΔE	-182.67	-182.68	-189.83	-190.01	-189.98	-190.84	-191.18	-191.16
\bar{M}	2.09	2.09	2.10	2.11	2.11	2.12	2.10	2.11

Hubbard U values of 0, 2, and 5 eV on Mn $3d$ orbitals. For both the orthorhombic and cubic phases, the tetrahedron method with Blöchl corrections was utilized to calculate the density of states (DOS) and total energies. All internal atomic positions were relaxed until the forces on atoms were smaller than 0.01 eV/Å.

III. RESULTS AND ANALYSIS

A recent experiment demonstrated that MnSe transforms to an orthorhombic phase (MnP-type structure, space group $Pnma$) at 30 GPa [29]. As illustrated in Fig. 1(a), the primitive cell of the orthorhombic-phase MnSe contains alternating corrugated Mn and Se layers, where the Mn and Se atoms form the edge-sharing $MnSe_6$ octahedra. The corresponding Brillouin zone (BZ) along with the high-symmetry \mathbf{k} points are schematically shown in Fig. 1(c). Figure 1(b) displays the exchange interactions between the Mn spins. As we can see, the nearest-neighboring (NN) J_1 is between the two Mn atoms of different layers within a unit cell, while the next-nearest-neighboring (NNN) J_2 is between the two Mn atoms in the same layer within a unit cell. The third NN J_3 and the fifth NN J_5 are between the two Mn atoms of the same layer in adjacent unit cells along the y direction, and the fourth NN J_4 is between the two Mn atoms from different layers in adjacent unit cells along the z direction. These exchange interactions will be used in the following analyses on the magnetic couplings.

We then studied the magnetic properties of the orthorhombic-phase MnSe. Firstly, we considered the nonmagnetic (NM) state, the ferromagnetic (FM) state, as well as several antiferromagnetic (AFM) states including the AFM1, AFM2, AFM3, AFM4, AFM5, and AFM6 states, whose spin configurations are shown in Fig. 2. The calculated relative energies of these magnetic states with respect to the NM state are listed in Table I. Clearly, the AFM3 state has the lowest energy among these states, while the energy difference between the AFM2 and AFM3 states is only 9.73 meV/Mn. For the other states, the energy differences are up to tens of meV/Mn. Focusing on the AFM2 and AFM3 states (Fig. 2), we find that their spin correlations along the x axis are both antiferromagnetic and those along the y axis are both ferromagnetic. The only difference between these two states lies in the form of spin correlation along the z axis: single-stripe (collinear) antiferromagnetic for the AFM2 state but ferromagnetic for the AFM3 state. Thus we conjectured that there should be a series of magnetic states

energetically between the AFM2 and AFM3 states. In all likelihood, the spin correlations along the x , y , and z axes of such magnetic states are antiferromagnetic, ferromagnetic, and staggered n -mer ($n > 1$), respectively. Here, the n -mer means that a set of n adjacent spins on a line are parallelly aligned. We calculated the energies of eight such n -mer states (Fig. 2), namely, dimer1 ($n = 2$), dimer2 ($n = 2$), trimer ($n = 3$), tetramer1 ($n = 4$), tetramer2 ($n = 4$), pentamer ($n = 5$), hexamer1 ($n = 6$), and hexamer2 ($n = 6$). As shown in Table I, the energy differences between the n -mer ($n = 2, 3, 4, 5, 6$) and AFM3 states are less than that between the AFM2 and AFM3 states. Specifically, the energies of the dimer1 (dimer2), trimer, tetramer1 (tetramer2), pentamer, hexamer1 (hexamer2) states are 9.35 (9.34), 2.19, 2.01 (2.04), 1.18, 0.84 (0.86) meV/Mn higher than that of the AFM3 state, respectively. And as n increases, the energy difference between the n -mer and AFM3 states decreases. It turns out that there are a large number of the quasidegenerate AFM states energetically. This is likely to induce strong antiferromagnetic fluctuations among the AFM3 state and the n -mer states with large n for the orthorhombic-phase MnSe.

In addition to the energies of various magnetic states for the orthorhombic-phase MnSe, the average local moments on Mn atoms are also listed in Table I. The calculated local moment on each Mn atom in MnSe at 30 GPa is about $2 \mu_B$, which is in accordance with the previous experimental findings that the Mn atom is on the verge of the intermediate-spin to low-spin states under 30 GPa [32]. The further calculations indicate that the local moment on each Mn atom reduces to $1.3 \mu_B$ at 35 GPa, approaching to a low-spin state [32]. These results verify our theoretical description of the magnetic interactions in the orthorhombic-phase MnSe under high pressure.

The above is the calculation results of magnetic properties of the orthorhombic-phase MnSe at the GGA level. Since Mn is a $3d$ element and the corresponding correlation is expected to play a crucial role, we also performed the corresponding calculations at the GGA + U level with the effective Hubbard U of 1 eV (Table II). It can be seen that the conclusion related to the orthorhombic-phase MnSe does not change qualitatively, that is, there may still exist AFM fluctuations in a small energy window (~ 7 meV/Mn). Meanwhile, the local moment on each Mn atom with the effective Hubbard U of 1 eV is up to about $2.8 \mu_B$, which is larger than that without the Hubbard U (Table I). Considering that there is no qualitative change in the conclusion, so next, we present the calculated results of the orthorhombic-phase MnSe at the GGA level without the Hubbard U .

TABLE II. Relative energies ΔE (in units of meV/Mn) of various magnetic states with respect to the NM state for the orthorhombic-phase MnSe calculated at the GGA + U level with an effective Hubbard U of 1 eV. The corresponding average local moments \bar{M} (in units of μ_B) on the Mn atoms are also listed.

State	NM	FM	AFM1	AFM2	AFM3	AFM4	AFM5	AFM6
ΔE	0.00	-364.46	-364.82	-485.38	-491.59	-362.94	-406.98	-454.61
\bar{M}	—	2.78	2.88	2.87	2.85	2.86	2.77	2.54
State	dimer1	dimer2	trimer	tetramer1	tetramer2	pentamer	hexamer1	hexamer2
ΔE	-472.63	-472.64	-482.89	-484.81	-484.80	-486.00	-487.16	-487.15
\bar{M}	2.85	2.85	2.83	2.85	2.85	2.85	2.85	2.85

To clarify the electronic properties of the orthorhombic-phase MnSe under high pressure, we present in Fig. 3 the band structure along the high-symmetry paths of the BZ, the density of states (DOS), as well as the Fermi surfaces for the AFM3 state, which is one of the most competing low-energy magnetic states for MnSe at 30 GPa (Table I). From the band structure [Fig. 3(a), left panel], we can see that there are several bands crossing the Fermi level with large dispersions, indicating a metallic behavior of the orthorhombic-phase MnSe. The calculated local DOS shown in the right panel of Fig. 3(a) indicates that the Mn-3*d* orbitals dominate around the Fermi level. Meanwhile, the Fermi surfaces displayed in Fig. 3(b) demonstrate the three-dimensional (3D) character of the electronic structure. There are one large electron-type pocket and one large hole-type pocket. And it should be noted that the small Fermi sheet [right panel in Fig. 3(b)] formed by the green band is not along the high-symmetry path [Fig. 3(a), left panel]. These electronic bands provide the itinerant car-

riers for superconductivity in the orthorhombic-phase MnSe under pressure.

IV. DISCUSSION AND SUMMARY

Magnetic interactions in magnetic systems can be quantified by the Heisenberg model. To describe the magnetic interactions among those Mn spins in the orthorhombic-phase MnSe, we employed an effective Heisenberg model,

$$H = -J_1 \sum_{\langle i,j \rangle} \vec{S}_i \cdot \vec{S}_j - J_2 \sum_{\langle\langle i,j \rangle\rangle} \vec{S}_i \cdot \vec{S}_j - J_3 \sum_{\langle\langle\langle i,j \rangle\rangle\rangle} \vec{S}_i \cdot \vec{S}_j - J_4 \sum_{\langle\langle\langle\langle i,j \rangle\rangle\rangle} \vec{S}_i \cdot \vec{S}_j - J_5 \sum_{\langle\langle\langle\langle\langle i,j \rangle\rangle\rangle} \vec{S}_i \cdot \vec{S}_j, \quad (1)$$

where $J_1, J_2, J_3, J_4,$ and J_5 denote the respective couplings between the nearest, the next-nearest, the third-nearest, the fourth-nearest, and the fifth-nearest neighboring Mn spins [Fig. 1(b)], and S is the local magnetic moment on Mn atom. Here $J < 0$ represents the AFM coupling between Mn spins, otherwise, it represents the FM coupling. The values of $J_1, J_2, J_3, J_4,$ and J_5 can be obtained via the energy differences among the AFM1, AFM2, AFM3, AFM4, AFM5, and AFM6 states. According to the calculated energy data (Table I), we obtain the values of $J_1, J_2, J_3, J_4,$ and J_5 , which are listed in Table III. The negative J_2 and positive J_3 account for the spin correlations along the x and y directions being antiferromagnetic and ferromagnetic, respectively.

Next, we show that the Heisenberg model Eq. (1) can effectively describe a variety of magnetic states in the orthorhombic-phase MnSe. According to Eq. (1), the energy formulas of the dimer1, dimer2, tetramer1, tetramer2, hexamer1, and hexamer2 states in their respective supercells can be expressed as

$$E_{\text{d}1} = 0J_1S^2 + 16J_2S^2 - 16J_3S^2 + 0J_4S^2 + 32J_5S^2, \quad (2)$$

$$E_{\text{d}2} = 0J_1S^2 + 16J_2S^2 - 16J_3S^2 + 0J_4S^2 + 32J_5S^2, \quad (3)$$

$$E_{\text{t}1} = -16J_1S^2 + 32J_2S^2 - 32J_3S^2 - 16J_4S^2 + 64J_5S^2, \quad (4)$$

TABLE III. Exchange couplings $J_1, J_2, J_3, J_4,$ and J_5 (in units of meV/ S^2) between the Mn spins calculated via the energy differences among the AFM1, AFM2, AFM3, AFM4, AFM5, and AFM6 states.

Exchange couplings	J_1	J_2	J_3	J_4	J_5
Value	6.2	-14.2	14.0	-3.7	-1.6

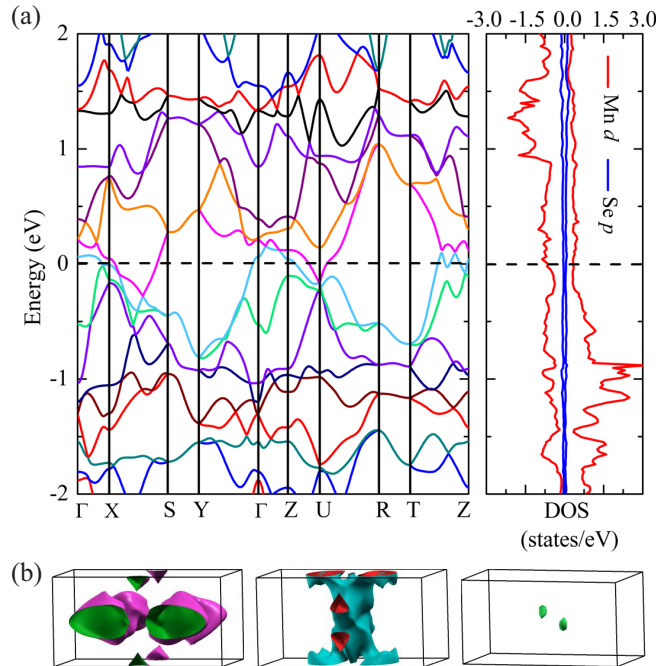


FIG. 3. (a) Band structure along the high-symmetry paths of the BZ and local density of states (DOS) for the AFM3 state of the orthorhombic-phase MnSe under 30 GPa. The Fermi energy is set to zero. (b) Fermi surfaces of the orthorhombic-phase MnSe in the AFM3 state at 30 GPa.

$$E_{\text{te}2} = -16J_1S^2 + 32J_2S^2 - 32J_3S^2 - 16J_4S^2 + 64J_5S^2, \quad (5)$$

$$E_{\text{he}1} = -32J_1S^2 + 48J_2S^2 - 48J_3S^2 - 32J_4S^2 + 96J_5S^2, \quad (6)$$

$$E_{\text{he}2} = -32J_1S^2 + 48J_2S^2 - 48J_3S^2 - 32J_4S^2 + 96J_5S^2. \quad (7)$$

Here $E_{\text{di}1}$, $E_{\text{di}2}$, $E_{\text{te}1}$, $E_{\text{te}2}$, $E_{\text{he}1}$, and $E_{\text{he}2}$ represent the energies of the dimer1, dimer2, tetramer1, tetramer2, hexamer1, and hexamer2 states, respectively. As we can see, the dimer1 and dimer2 states have the same energy formulas, as do the tetramer1 and tetramer2 states, as well as the hexamer1 and hexamer2 states. These agree with our calculated results that $E_{\text{dimer}1} = E_{\text{dimer}2}$, $E_{\text{tetramer}1} = E_{\text{tetramer}2}$, and $E_{\text{hexamer}1} = E_{\text{hexamer}2}$, as shown in Table I. In addition, according to the above model, the energy sequence from high to low among the AFM2, AFM3, dimer1/2, trimer, tetramer1/2, pentamer, hexamer1/2, $E_{\text{AFM}3}$ when $J_1 > -J_4$. The derived values of J_1 and J_4 satisfy this inequation, also consistent with the calculated results that there are a series of staggered n -mer AFM states whose energies are between those of the AFM2 and AFM3 states and the energies of these n -mer states decrease and approach to that of the AFM3 state with increasing n , namely these AFM states are energetically in quasidegeneracy. Actually, along z axis any combinations of staggered n -mers basically give the similar energies [43]. All of the above analyses show that the magnetic interactions among these magnetic states we considered in the orthorhombic-phase MnSe can be described by the effective Heisenberg model.

The above exchange couplings J that we obtained for the effective Heisenberg model of MnSe have the following significances. They can serve as a reference for the neutron scattering experimentalists to fit the spin wave spectra [44] and for the high-field magnetometry researchers to estimate the field strength to suppress the antiferromagnetism. Meanwhile, they can also be adopted in a high-temperature coupled cluster expansion of the model, which provides insights in the understanding of the measured susceptibility and specific heat for the paramagnetic phase.

At present, the proposed mechanisms for unconventional superconductivity include Fermi surface nesting [45–47], electron-phonon coupling (EPC) [48], spin fluctuations [49], etc. From Fig. 3(b), it can be seen that there is no Fermi surface nesting in the orthorhombic-phase MnSe, which rules out the Fermi surface nesting as a potential superconducting mechanism. In addition, we performed the EPC calculations for the orthorhombic-phase MnSe at 30 GPa via Quantum ESPRESSO (QE) package [50], so as to examine the importance of EPC mechanism. However, it is found that the maximum value of mode-resolved EPC constant does not exceed 0.25 for each specific \mathbf{q} point, which indicates that the EPC strength in the orthorhombic-phase MnSe is too weak to yield the experimental T_c of about 5.8 ~ 8 K at 30 GPa [29]. Similar to our previous findings in bulk β -FeSe [43], α -RuCl₃ [51], and LiV₂O₄ [52] in which there exist a

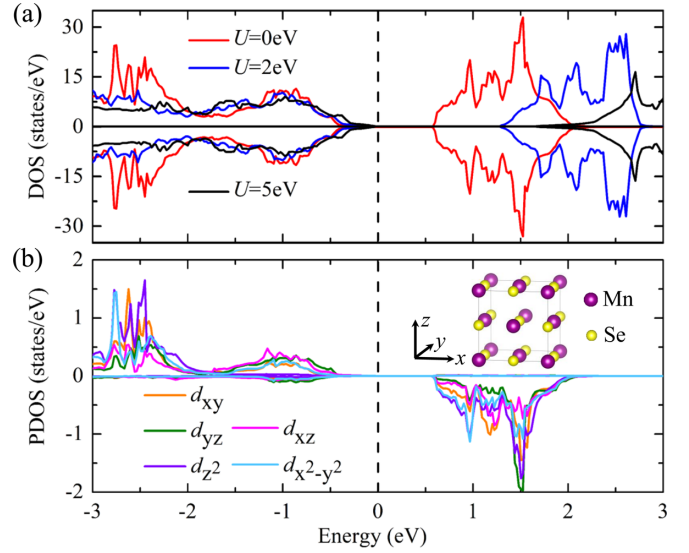


FIG. 4. (a) Total DOS for the cubic-phase (NaCl-type) MnSe at ambient pressure calculated with the effective Hubbard U values of 0, 2, and 5 eV. (b) Partial DOS (PDOS) of the Mn atom in the cubic-phase MnSe calculated with $U = 0$ eV. The Fermi level is set to zero. Inset shows the crystal structure of the cubic phase.

series of almost degenerate low-lying magnetic states, here the AFM3 state and a series of staggered n -mer AFM states are energetically quasidegenerated in the orthorhombic-phase MnSe, which may induce strong AFM fluctuations like in bulk β -FeSe [43]. This kind of magnetic instability potentially can play a role in superconductivity of the orthorhombic-phase MnSe, as in cuprate and iron-based superconductors [53–60].

In summary, we have investigated the magnetic and electronic properties of the orthorhombic-phase MnSe under high pressure via the first-principles electronic structure calculations. Our calculations show that there may exist strong antiferromagnetic fluctuations in a narrow energy window (less than 3 meV/Mn) among the AFM3 state and a series of staggered n -mer AFM states that we named, including the hexamer1 ($n = 6$), hexamer2 ($n = 6$), pentamer ($n = 5$), tetramer1 ($n = 4$), tetramer2 ($n = 4$), and trimer ($n = 3$) states. These n -mer states are such states that the spin correlations along the x , y , and z axes show AFM, FM, and staggered n -mer AFM couplings, respectively. The larger n is, the closer the energy of the n -mer state is to that of the AFM3 state. Moreover, the moderate local moments on the Mn atoms for the metallic orthorhombic phase of MnSe under high pressure, rather than the high-spin state in the insulating cubic phase of MnSe at ambient pressure (see Appendix), can benefit to the spin fluctuations, which potentially may be related to the superconducting mechanism of the orthorhombic-phase MnSe.

ACKNOWLEDGMENTS

We thank H.-C. Yang for helpful discussions. This work was supported by the National Key R&D Program of China (Grants No. 2017YFA0302903 and No. 2019YFA0308603), the National Natural Science Foundation of China (Grants No. 12174443 and No. 11934020), the Beijing Natural Science

Foundation (Grant No. Z200005), the CAS Interdisciplinary Innovation Team, the Fundamental Research Funds for the Central Universities, and the Research Funds of Renmin University of China (Grant No. 19XNLG13). Computational resources were provided by the Physical Laboratory of High Performance Computing at Renmin University of China.

APPENDIX

The crystal structure of MnSe undergoes several complicated changes with the applied pressure [29]. Apart from the above orthorhombic phase under high pressure, MnSe is in

the cubic phase (NaCl-type structure) at ambient pressure, as illustrated in the inset of Fig. 4(b). From the total DOS [Fig. 4(a)] calculated with the addition of effective Hubbard U ($U = 0, 2, \text{ and } 5 \text{ eV}$) and the magnetic structure determined by neutron powder diffraction (NPD) measurement [41], we can see that the cubic-phase MnSe is semiconducting at ambient pressure, which is consistent with the previous experiment [31] and calculations [61,62]. According to the partial DOS (PDOS) in Fig. 4(b), the five Mn-3d orbitals are all half occupied, also in accordance with the previously suggested high-spin state ($S = 5/2$) of Mn^{2+} in the cubic phase [32].

-
- [1] M. S. Torikachvili, S. L. Bud'ko, N. Ni, and P. C. Canfield, *Phys. Rev. Lett.* **101**, 057006 (2008).
- [2] T. Park, E. Park, H. Lee, T. Klimczuk, E. D. Bauer, F. Ronning, and J. D. Thompson, *J. Phys.: Condens. Matter* **20**, 322204 (2008).
- [3] P. L. Alireza, Y. T. C. Ko, J. Gillett, C. M. Petrone, J. M. Cole, G. G. Lonzarich, and S. E. Sebastian, *J. Phys.: Condens. Matter* **21**, 012208 (2009).
- [4] M. Kumar, M. Nicklas, A. Jesche, N. Caroca-Canales, M. Schmitt, M. Hanfland, D. Kasinathan, U. Schwarz, H. Rosner, and C. Geibel, *Phys. Rev. B* **78**, 184516 (2008).
- [5] A. S. Sefat, R.-Y. Jin, M. A. McGuire, B. C. Sales, D. J. Singh, and D. Mandrus, *Phys. Rev. Lett.* **101**, 117004 (2008).
- [6] S. Sharma, A. Bharathi, S. Chandra, V. R. Reddy, S. Paulraj, A. T. Satya, V. S. Sastry, A. Gupta, and C. S. Sundar, *Phys. Rev. B* **81**, 174512 (2010).
- [7] N. Ni, A. Thaler, A. Kracher, J.-Q. Yan, S. L. Bud'ko, and P. C. Canfield, *Phys. Rev. B* **80**, 024511 (2009).
- [8] L.-J. Li, Y.-K. Luo, Q.-B. Wang, H. Chen, Z. Ren, Q. Tao, Y.-K. Li, X. Lin, M. He, Z.-W. Zhu, G.-H. Cao, and Z.-A. Xu, *New J. Phys.* **11**, 025008 (2009).
- [9] S. R. Saha, T. Drye, K. Kirshenbaum, N. P. Butch, P. Y. Zavalij, and J. Paglione, *J. Phys.: Condens. Matter* **22**, 072204 (2010).
- [10] A. Leithe-Jasper, W. Schnelle, C. Geibel, and H. Rosner, *Phys. Rev. Lett.* **101**, 207004 (2008).
- [11] A. S. Sefat, A. Huq, M. A. McGuire, R.-Y. Jin, B. C. Sales, D. Mandrus, L. M. D. Cranswick, P. W. Stephens, and K. H. Stone, *Phys. Rev. B* **78**, 104505 (2008).
- [12] R. J. Birgeneau, C. Stock, J. M. Tranquada, and K. Yamada, *J. Phys. Soc. Jpn.* **75**, 111003 (2006).
- [13] D. Vaknin, S. K. Sinha, D. E. Moncton, D. C. Johnston, J. M. Newsam, C. R. Safinya, and H. E. King, *Phys. Rev. Lett.* **58**, 2802 (1987).
- [14] J. M. Tranquada, D. E. Cox, W. Kunmann, H. Moudden, G. Shirane, M. Suenaga, P. Zolliker, D. Vaknin, S. K. Sinha, M. S. Alvarez, A. J. Jacobson, and D. C. Johnston, *Phys. Rev. Lett.* **60**, 156 (1988).
- [15] P. A. Lee, N. Nagaosa, and X.-G. Wen, *Rev. Mod. Phys.* **78**, 17 (2006).
- [16] J. Paglione and R. L. Greene, *Nat. Phys.* **6**, 645 (2010).
- [17] P.-C. Dai, J.-P. Hu, and E. Dagotto, *Nat. Phys.* **8**, 709 (2012).
- [18] P.-C. Dai, *Rev. Mod. Phys.* **87**, 855 (2015).
- [19] A. I. Goldman, D. N. Argyriou, B. Ouladdiaf, T. Chatterji, A. Kreyssig, S. Nandi, N. Ni, S. L. Bud'ko, P. C. Canfield, and R. J. McQueeney, *Phys. Rev. B* **78**, 100506(R) (2008).
- [20] C. de la Cruz, Q. Huang, J. W. Lynn, J.-Y. Li, W. R. II, J. L. Zarestky, H. A. Mook, G.-F. Chen, J.-L. Luo, N.-L. Wang, and P.-C. Dai, *Nature (London)* **453**, 899 (2008).
- [21] Q. Huang, Y. Qiu, W. Bao, M. A. Green, J. W. Lynn, Y. C. Gasparovic, T. Wu, G. Wu, and X.-H. Chen, *Phys. Rev. Lett.* **101**, 257003 (2008).
- [22] S.-L. Li, C. de la Cruz, Q. Huang, G.-F. Chen, T.-L. Xia, J.-L. Luo, N.-L. Wang, and P.-C. Dai, *Phys. Rev. B* **80**, 020504(R) (2009).
- [23] M. Rotter, M. Tegel, and D. Johrendt, *Phys. Rev. Lett.* **101**, 107006 (2008).
- [24] Y. Kamihara, T. Watanabe, M. Hirano, and H. Hosono, *J. Am. Chem. Soc.* **130**, 3296 (2008).
- [25] J.-G. Cheng, K. Matsubayashi, W. Wu, J.-P. Sun, F.-K. Lin, J.-L. Luo, and Y. Uwatoko, *Phys. Rev. Lett.* **114**, 117001 (2015).
- [26] M. D. Banus, *J. Solid State Chem.* **4**, 391 (1972).
- [27] Y.-J. Xu, M. Liu, P. Zheng, X.-R. Chen, J.-G. Cheng, J.-L. Luo, W.-H. Xie, and Y.-F. Yang, *J. Phys.: Condens. Matter* **29**, 244001 (2017).
- [28] P. Bonfá, I. J. Onuorah, and R. D. Renzi, [arXiv:1603.08891](https://arxiv.org/abs/1603.08891).
- [29] T.-L. Hung, C.-H. Huang, L.-Z. Deng, M.-N. Ou, Y.-Y. Chen, M.-K. Wu, S.-Y. Huyan, C.-W. Chu, P.-J. Chen, and T.-K. Lee, *Nat. Commun.* **12**, 5436 (2021).
- [30] C. H. Leung, *J. Am. Ceram. Soc.* **62**, 613 (1979).
- [31] H. Sato, T. Mihara, A. Furuta, M. Tamura, K. Mimura, N. Happono, M. Taniguchi, and Y. Ueda, *Phys. Rev. B* **56**, 7222 (1997).
- [32] Y.-G. Wang, L.-G. Bai, T. Wen, L.-X. Yang, H.-Y. Gou, Y.-M. Xiao, P. Chow, M. Pravica, W.-G. Yang, and Y.-S. Zhao, *Angew. Chem. Int. Ed.* **55**, 10350 (2016).
- [33] G. Kresse and D. Joubert, *Phys. Rev. B* **59**, 1758 (1999).
- [34] P. E. Blöchl, *Phys. Rev. B* **50**, 17953 (1994).
- [35] G. Kresse and J. Furthmüller, *Comput. Mater. Sci.* **6**, 15 (1996).
- [36] G. Kresse and J. Hafner, *Phys. Rev. B* **47**, 558 (1993).
- [37] G. Kresse and J. Furthmüller, *Phys. Rev. B* **54**, 11169 (1996).
- [38] J. P. Perdew, K. Burke, and M. Ernzerhof, *Phys. Rev. Lett.* **77**, 3865 (1996).
- [39] N. Marzari, A. A. Mostofi, J. R. Yates, I. Souza, and D. Vanderbilt, *Rev. Mod. Phys.* **84**, 1419 (2012).

- [40] A. A. Mostofi, J. R. Yates, G. Pizzi, Y.-S. Lee, I. Souza, D. Vanderbilt, and N. Marzari, *Comput. Phys. Commun.* **185**, 2309 (2014).
- [41] C.-H. Huang, C.-W. Wang, C.-C. Chang, Y.-C. Lee, G.-T. Huang, M.-J. Wang, and M.-K. Wu, *J. Magn. Magn. Mater.* **483**, 205 (2019).
- [42] S. L. Dudarev, G. A. Botton, S. Y. Savrasov, C. J. Humphreys, and A. P. Sutton, *Phys. Rev. B* **57**, 1505 (1998).
- [43] K. Liu, Z.-Y. Lu, and T. Xiang, *Phys. Rev. B* **93**, 205154 (2016).
- [44] F. Ye, R. S. Fishman, J. A. Fernandez-Baca, A. A. Podlesnyak, G. Ehlers, H. A. Mook, Y.-Q. Wang, B. Lorenz, and C. W. Chu, *Phys. Rev. B* **83**, 140401(R) (2011).
- [45] K. Terashima, Y. Sekiba, J. H. Bowen, K. Nakayama, T. Kawahara, T. Sato, P. Richard, Y.-M. Xu, L.-J. Li, G.-H. Cao, Z.-A. Xu, H. Ding, and T. Takahashi, *Proc. Natl. Acad. Sci. USA* **106**, 7330 (2009).
- [46] H. Ding, P. Richard, K. Nakayama, K. Sugawara, T. Arakane, Y. Sekiba, A. Takayama, S. Souma, T. Sato, T. Takahashi, Z. Wang, X. Dai, Z. Fang, G.-F. Chen, J.-L. Luo, and N.-L. Wang, *Europhys. Lett.* **83**, 47001 (2008).
- [47] C. Liu, G. D. Samolyuk, Y. Lee, N. Ni, Takeshi Kondo, A. F. Santander-Syro, S. L. Bud'ko, J. L. McChesney, E. Rotenberg, T. Valla, A. V. Fedorov, P. C. Canfield, B. N. Harmon, and A. Kaminski, *Phys. Rev. Lett.* **101**, 177005 (2008).
- [48] X.-Y. Chong, Y.-H. Jiang, R. Zhou, and J. Feng, *Sci. Rep.* **6**, 21821 (2016).
- [49] N. Nagaosa, *Science* **275**, 1078 (1997).
- [50] P. Giannozzi, S. Baroni, N. Bonini, M. Calandra, R. Car, C. Cavazzoni, D. Ceresoli, G. L. Chiarotti, M. Cococcioni, I. Dabo *et al.*, *J. Phys.: Condens. Matter* **21**, 395502 (2009).
- [51] H.-C. Yang, B.-C. Gong, K. Liu, and Z.-Y. Lu, *J. Phys.: Condens. Matter* **31**, 025803 (2019).
- [52] B.-C. Gong, H.-C. Yang, K. Jin, K. Liu, and Z.-Y. Lu, *Chin. Phys. B* **29**, 077508 (2020).
- [53] M. Fujita, H. Hiraka, M. Matsuda, M. Matsuura, J. M. Tranquada, S. Wakimoto, G.-Y. Xu, and K. Yamada, *J. Phys. Soc. Jpn.* **81**, 011007 (2012).
- [54] K. Ueda, T. Moriya, and Y. Takahashi, *J. Phys. Chem. Solids* **53**, 1515 (1992).
- [55] P. Monthoux and D. Pines, *Phys. Rev. B* **47**, 6069 (1993).
- [56] S. Nakamura, T. Moriya, and K. Ueda, *J. Phys. Soc. Jpn.* **65**, 4026 (1996).
- [57] I. I. Mazin, D. J. Singh, M. D. Johannes, and M. H. Du, *Phys. Rev. Lett.* **101**, 057003 (2008).
- [58] K. Kuroki, S. Onari, R. Arita, H. Usui, Y. Tanaka, H. Kontani, and H. Aoki, *Phys. Rev. Lett.* **101**, 087004 (2008).
- [59] C. H. Lee, K. Kihou, H. Kawano-Furukawa, T. Saito, A. Iyo, H. Eisaki, H. Fukazawa, Y. Kohori, K. Suzuki, H. Usui, K. Kuroki, and K. Yamada, *Phys. Rev. Lett.* **106**, 067003 (2011).
- [60] J.-H. Zhang, R. Sknepnek, and J. Schmalian, *Phys. Rev. B* **82**, 134527 (2010).
- [61] P. Amiri, S. J. Hashemifar, and H. Akbarzadeh, *Phys. Rev. B* **83**, 165424 (2011).
- [62] W.-Q. Zhou, S.-X. Wu, and S.-W. Li, *J. Magn. Magn. Mater.* **395**, 166 (2015).